

ELECTRONIC SUPPLEMENTARY INFORMATION

Selective n-propanol formation from CO₂ over degradation-resistant activated PdCu alloy foam electrocatalysts

Motiar Rahaman,^{* ‡ §} Kiran Kiran,[‡] Ivan Zelocualtecatl Montiel, Vitali Grozovski, Abhijit Dutta,^{*} and Peter Broekmann^{*}

Department of Chemistry and Biochemistry, University of Bern, Freiestrasse 3, 3012 Bern, Switzerland

^{*}Corresponding authors: mr820@cam.ac.uk, abhijit.dutta@dcb.unibe.ch, and peter.broekmann@dcb.unibe.ch

[‡] These authors contributed equally to this work.

[§] Current address: *Department of Chemistry, University of Cambridge, Lensfield Road, CB2 1EW Cambridge, United Kingdom.*

Fig. S1

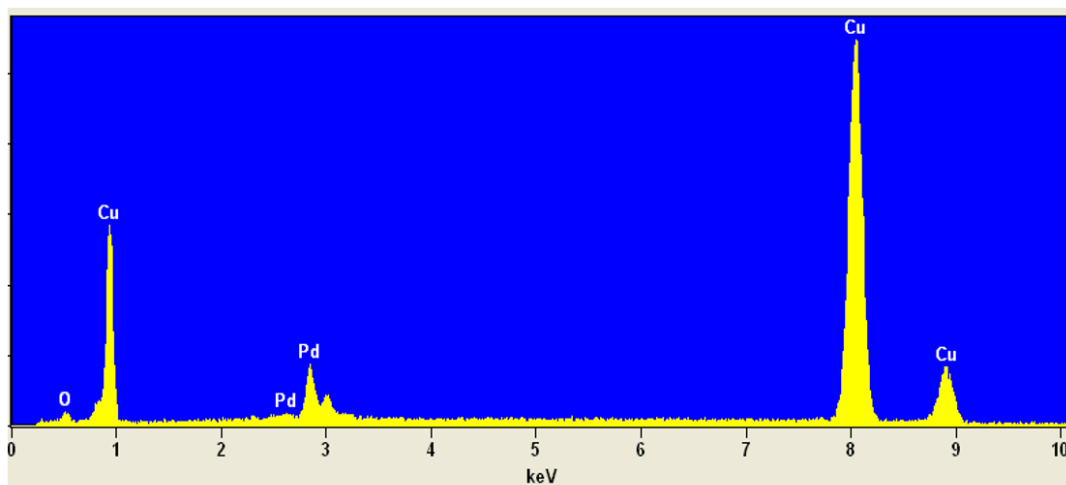


Fig. S1 Elemental EDX analysis of the *as-prepared* PdCu foam catalyst: A representative EDX spectra of the *ap*-PdCu catalyst material shows the presence of Cu (93 at%) and Pd (7 at%).

Fig. S2

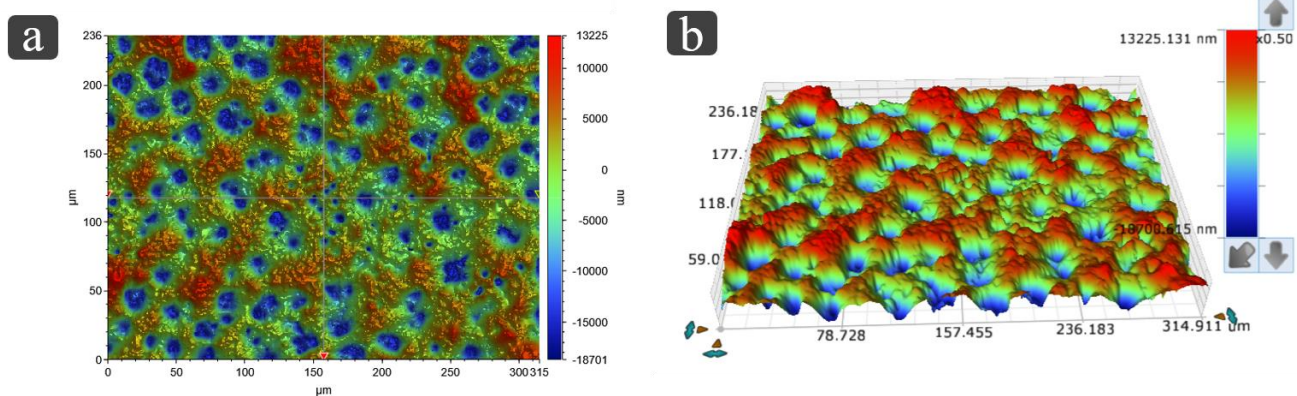


Fig. S2 White light interferometry (WLI) analysis of the *ap*-Pd₉Cu₉₁ catalyst. a) Top-down view (2D); b) Corresponding 3D representation of the WLI image. For the electrodeposited alloy foam a depth of $\sim 25 \pm 2 \mu\text{m}$ was determined on the basis of the WLI analysis.

Fig. S3

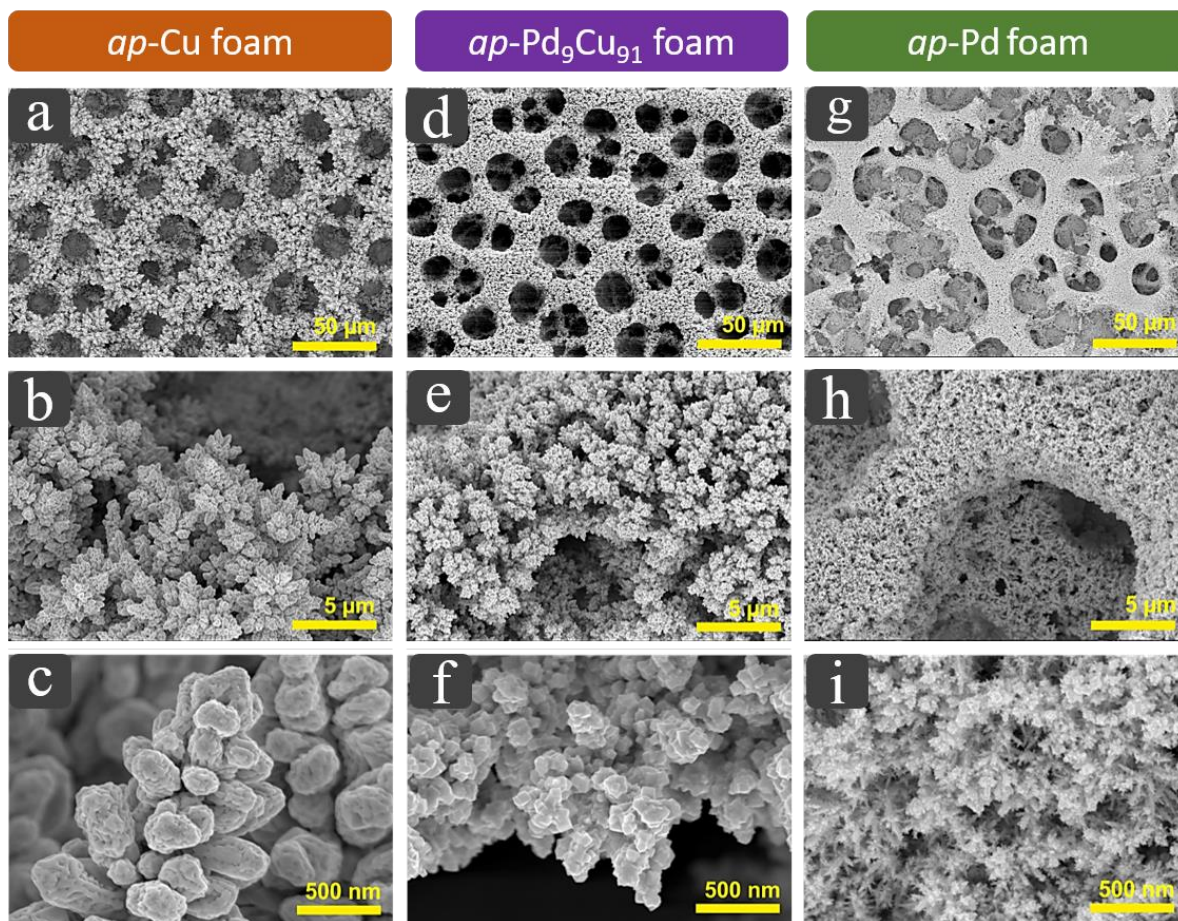


Fig. S3 SEM and HR-SEM analysis of the pure Cu foam (a, b, c), the *as-prepared* Pd₉Cu₉₁ foam (d, e, f) and the pure Pd foam (g, h, i). Important to note is that Pd does not form a compact mesoporous foam structure, at least under the applied deposition conditions (-3A cm⁻², 40s).

Fig. S4

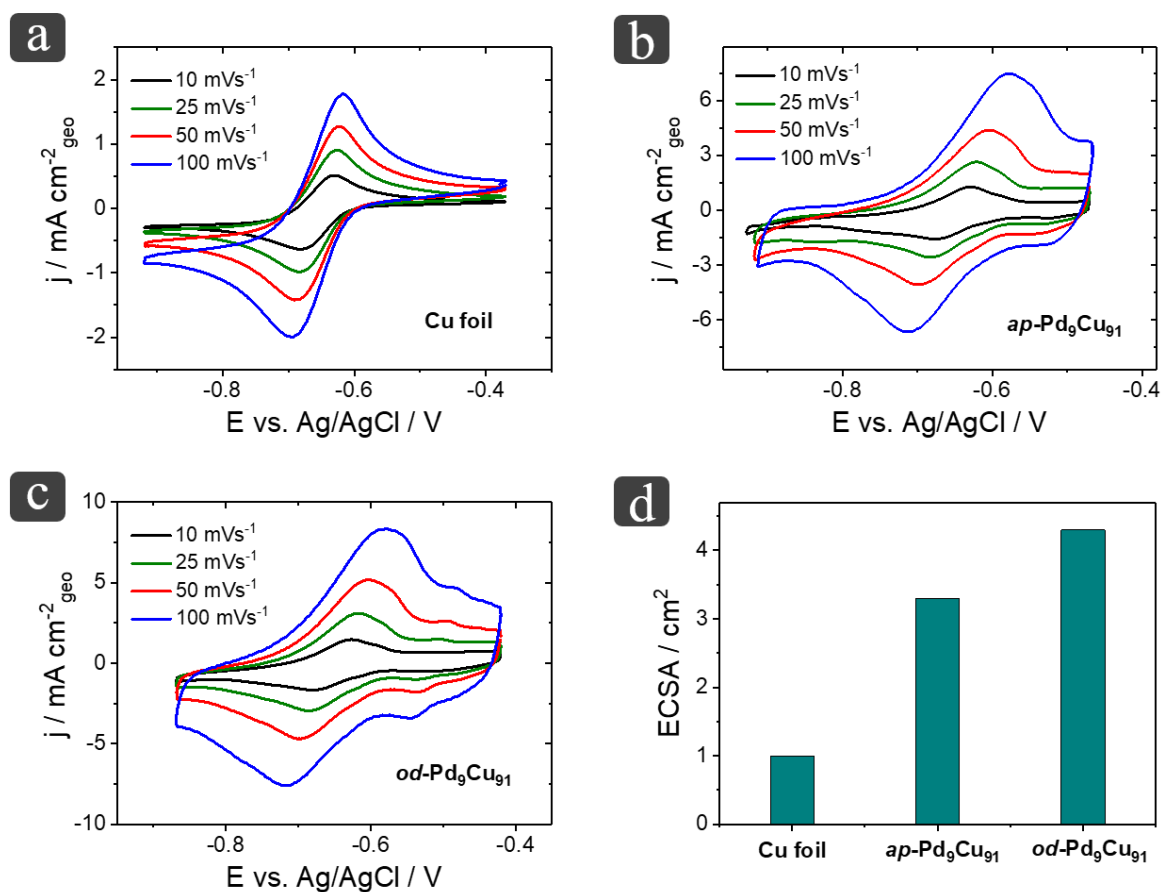


Fig. S4 Scan rate dependent voltammograms of (a) the Cu foil substrate, (b) the $ap\text{-Pd}_9\text{Cu}_{91}$ catalyst deposited on the Cu foil, and (c) the respective $od\text{-Pd}_9\text{Cu}_{91}$ catalyst. Aqueous 1M Na_2SO_4 (ACS grade, Sigma Aldrich) solution was used as an electrolyte. 10 mM di-methyl viologen di-chloride (DMVCl_2 , ACS grade, Sigma Aldrich) was added to the electrolyte as the reversible redox-probe. The electrochemically active surface area (ECSA) of the catalysts was determined on the basis of the Randles-Sevcik equation. (d) A comparison of ECSAs obtained from the viologen method (Cu foil: 1 cm^2 , $ap\text{-Pd}_9\text{Cu}_{91}$: 3.3 cm^2 , and $od\text{-Pd}_9\text{Cu}_{91}$: 4.3 cm^2).

Fig. S5

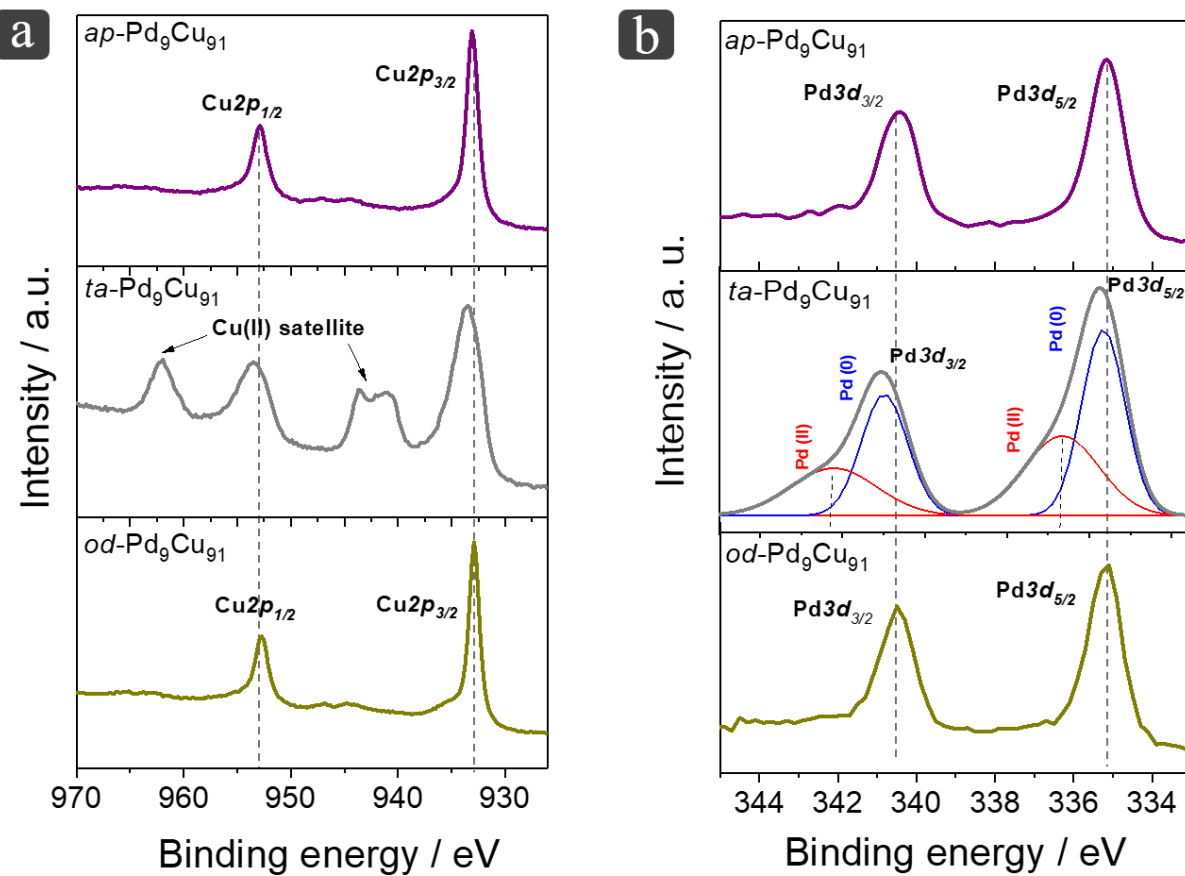


Fig. S5 *Ex situ* XPS analysis of the *ap*-Pd₉Cu₉₁, *ta*-Pd₉Cu₉₁, and *od*-Pd₉Cu₉₁ samples. Panel (a) and panel (b) show the respective Cu and the Pd regions.

Fig. S6

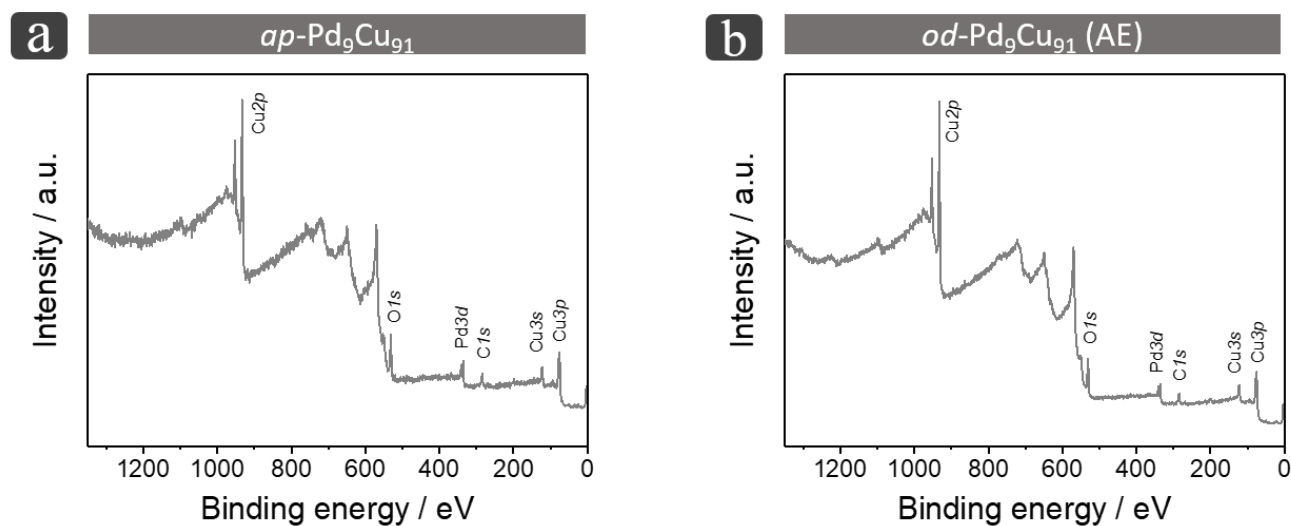


Fig. S6 Survey XPS spectra of the (a) *ap*-Pd₉Cu₉₁ and (b) the *od*-Pd₉Cu₉₁ sample after 3 h CO₂RR at -0.65 V vs. RHE. These XPS results suggest that there are no metallic contaminations (e.g. Pt) present on the catalyst surface after the electrolysis which might originate from an anodic dissolution of the anode material during the initial foam deposition or the subsequent CO₂ electrolysis.

From this it can be concluded that the electrolysis data are not impaired by metallic impurities which might influence the resulting product distribution.

Fig. S7

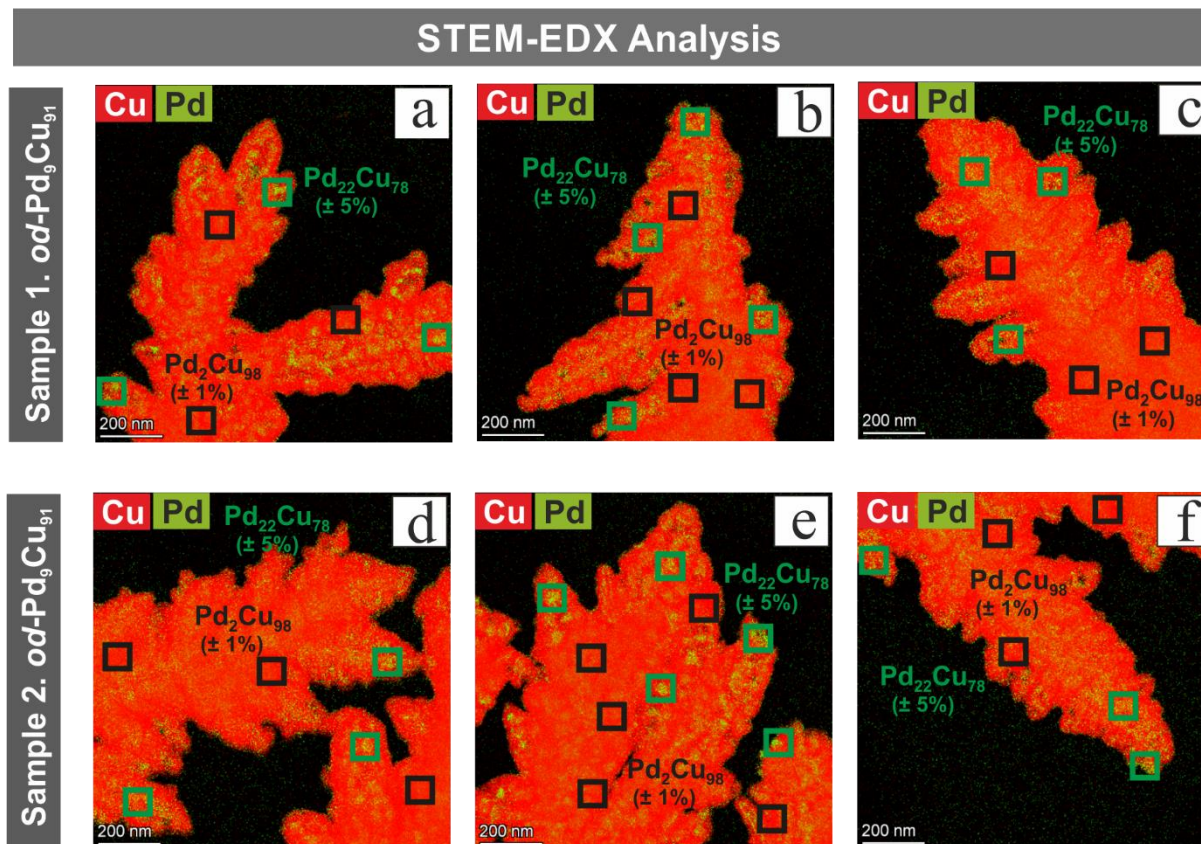


Fig. S7 High-resolution STEM-EDX analyses of two different $od-Pd_9Cu_{91}$ catalyst samples demonstrating the high reproducibility of the combined deposition and activation approach applied herein.

(a-c) Three selected spots of sample 1; (d-f) three selected spots of sample 2. Black and green frames highlight Cu-rich and Pd-rich domains, respectively. According to the (quasi)quantitative EDX analysis, the Cu-rich domains contain $\sim 98\%$ Cu and $\sim 2\%$ Pd (spatial scattering of $\pm 1\%$). Pd-rich domains are composed of $\sim 78\%$ Cu and $\sim 22\%$ Pd (spatial scattering of $\pm 5\%$).

Fig. S8

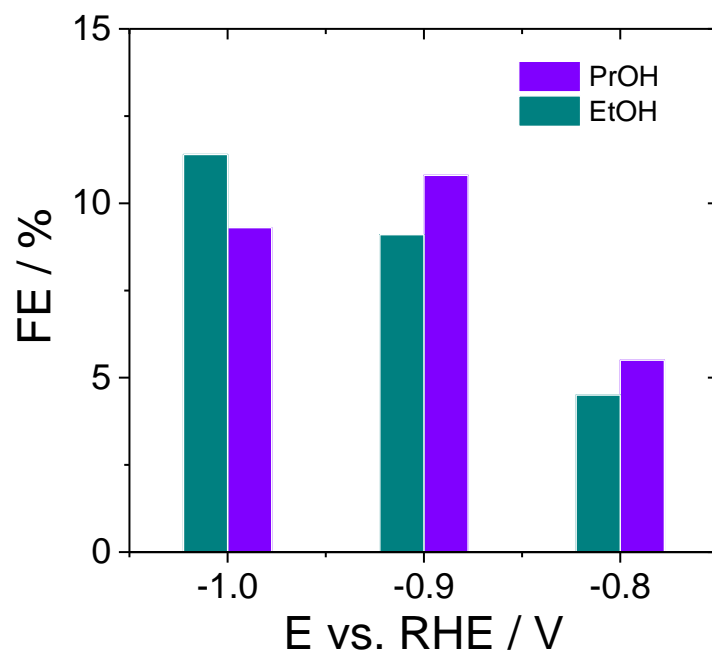


Fig. S8 Product selectivity of the potentiostatic CO₂ electrolysis carried out over an oxide-derived (pure) Cu foam catalyst. Similar procedure was used to prepare and activate the catalyst. (Deposition conditions: 0.025 M CuSO₄·5H₂O in 1.5 M H₂SO₄, -3 A cm⁻² for 40s. Annealing condition: 200°C for 12 h in air)

Fig. S9

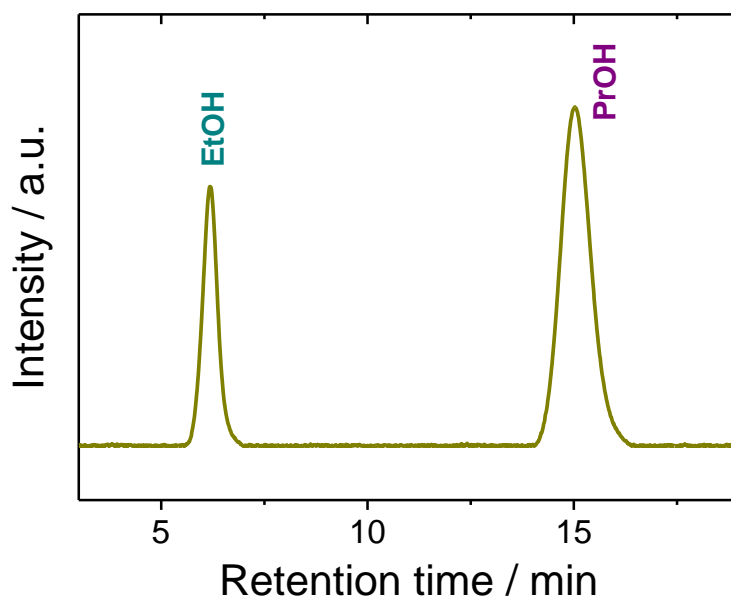


Fig. S9 Representative gas chromatogram from the long-term electrolysis experiment at -0.65V vs. RHE using the *od*-Pd₉Cu₉ foam as a catalyst. The chromatogram was recorded by an FID detector after 20 h of electrolysis.

Fig. S10

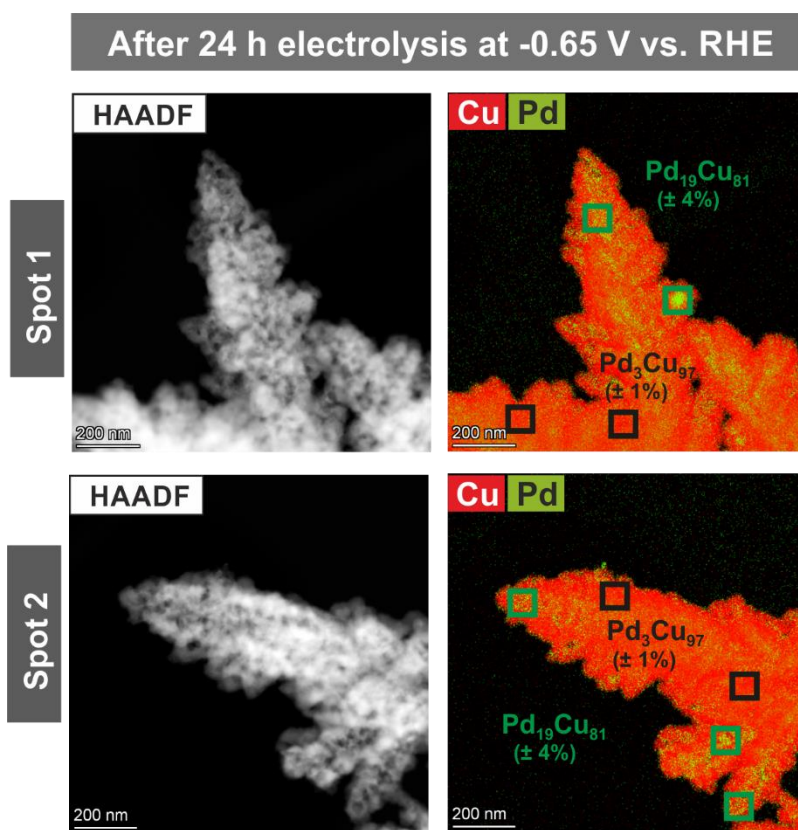


Fig. S10 HAADF and STEM-EDX analyses of the *od*-Pd₉Cu₉₁ catalyst after 24 h electrolysis at -0.65 V vs. RHE. It is clearly visible that the Cu-rich and Pd-rich domains are still separated on the binary foam catalyst after the electrolysis.

Fig. S11

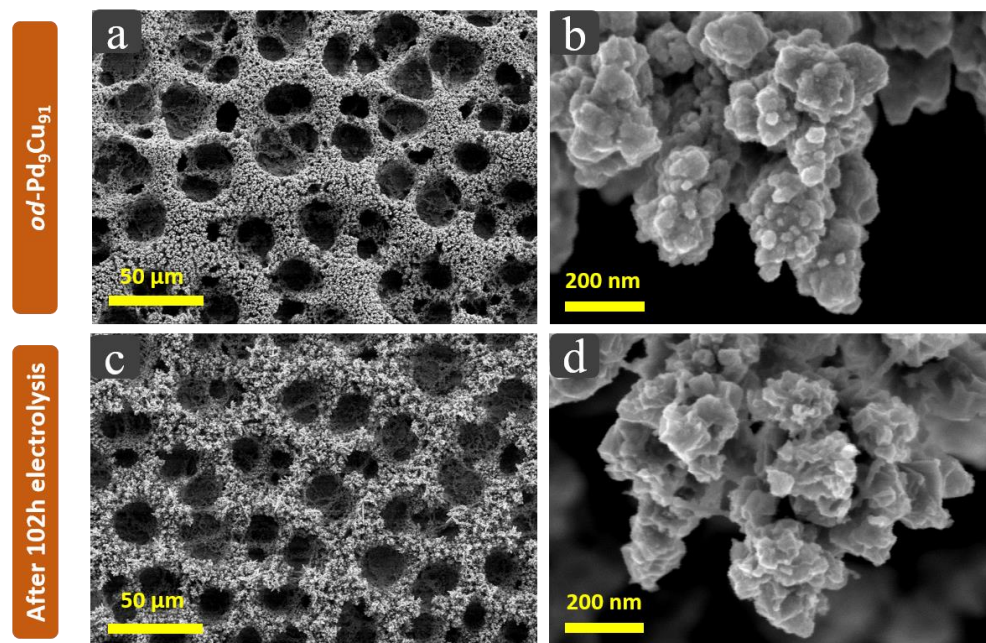


Fig. S11 (a, b) SEM and HR-SEM analysis of the *od*-Pd₉Cu₉₁ catalyst. (c, d) The same catalyst after 102 h of CO₂RR at -0.65 V vs. RHE. The mesoporous morphology of the oxide-derived catalyst is still intact after the 102 h electrolysis. The overall roughness seems, however, to be increased.

Fig. S12

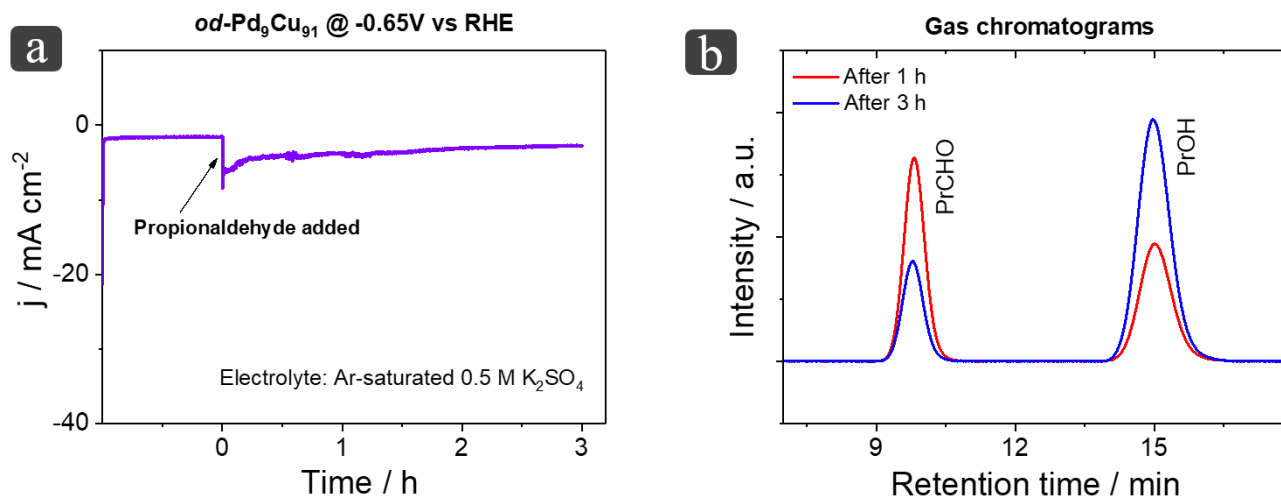


Fig. S12 Control experiment using propionaldehyde (750 ppm CH₃CH₂CHO) as the reactant in a (CO₂/bicarbonate)-free electrolyte (Ar-saturated 0.5M K₂SO₄) and the *od*-Pd₉Cu₉₁ material as the catalyst. The n-propanol (ProOH) formation at -0.65V vs RHE was monitored as function of time. A sudden increase of negative current density was observed immediately after injecting the aldehyde to the electrolyte. (a) Current density (j) vs. time trace of the electrolysis experiment; (b) representative gas chromatograms demonstrating the formation of ProOH during electrolysis.

These results support the hypothesis that propionaldehyde is the key intermediate of the n-propanol formation.

Fig. S13

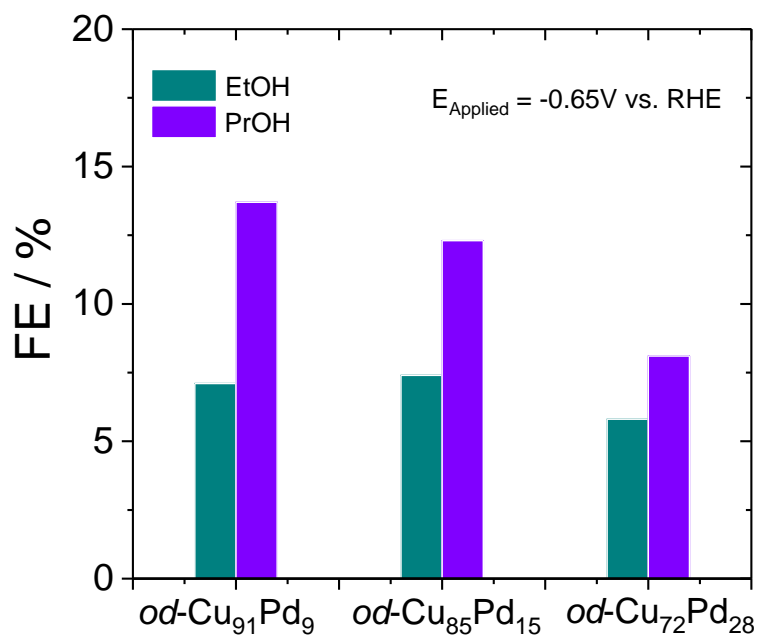


Fig. S13. A composition dependence activity of Cu-Pd alloy towards alcohol production. As prepared Pd_9Cu_{91} alloy, $Pd_{15}Cu_{85}$ alloy, and $Pd_{28}Cu_{72}$ alloys were activated by similar thermal annealing and subsequent electrochemical treatment. It was observed that with increasing Pd content in the as-prepared catalysts, the activity and selectivity of C3 alcohol production was gradually decreasing on their corresponding activated oxide-derived catalysts. The applied potential was $-0.65V$ vs. RHE.

Table S1. Average faradaic efficiencies of different products obtained from potentiostatic CO₂ electrolysis experiments over the *ap*-Pd₉Cu₉₁ catalyst. Note that only negligible amounts of EtOH and n-PrOH (maximum total efficiency ~5 %) were observed on the as-prepared catalyst material.

E vs. RHE	FE_{CO} (%)	FE_{H₂} (%)	FE_{HCOO⁻} (%)	FE_{C₂H₄} (%)	FE_{C₂H₆} (%)
-0.45	35.6	29.9	34.8	-	-
-0.55	27.3	27.4	42.7	-	-
-0.65	15.6	37.9	35.1	6.1	3.3
-0.75	6.5	49.0	26.3	8.2	4.1
-0.85	2.0	64.9	17.5	6.0	3.5
-0.95	1.5	72.8	12.5	3.5	2.1

Table S2. Average faradaic efficiencies of different products obtained from potentiostatic CO₂ electrolysis experiments on the *od*-Pd₉Cu₉₁ catalyst.

E vs. RHE	FE_{CO} (%)	FE_{H₂} (%)	FE_{HCOO⁻} (%)	FE_{C₂H₄} (%)	FE_{C₂H₆} (%)	FE_{EtOH} (%)	FE_{PrOH} (%)
-0.45	25.8	36.7	22.9	-	-	3.0	4.7
-0.55	18.3	33.0	26.8	1.7	2.1	6.3	10.4
-0.65	4.6	44.5	12.4	5.5	6.7	7.1	13.7
-0.75	2.1	49.1	7.1	7.8	11.6	8.0	12.2
-0.85	1.1	63.8	4.3	6.7	8.5	6.4	8.2
-0.95	0.6	75.9	2.7	4.3	5.4	3.3	4.1

Table S3. Literature survey: Faradaic efficiency (FE) and current efficiency (CE) data of n-propanol (PrOH) and ethanol (EtOH) production during CO₂ electroreduction over various Cu and Cu-based materials. Best PrOH forming catalysts are listed below.

Catalyst Material	FE_{PrOH} (%) CE_{PrOH} (mA cm⁻²)	FE_{EtOH} (%) CE_{EtOH} (mA cm⁻²)	C3 Selectivity	E range (V vs. RHE)	Reference
Phase separated <i>od</i> -Pd ₉ Cu ₉₁	FE _{PrOH} : 13.7% CE _{PrOH} : -1.15 mA cm ⁻²	FE _{EtOH} : 7.1% CE _{EtOH} : -0.60 mA cm ⁻²	~2	-0.65V	This Work
Agglomerated Cu nanocrystals	FE _{PrOH} : 10.58% CE _{PrOH} : -1.497 mA cm ⁻²	FE _{EtOH} : 7.70% CE _{EtOH} : -1.091 mA cm ⁻²	~1.4	-0.85V	1
Cu ²⁺ ion cycled Cu	FE _{PrOH} : 15%	FE _{EtOH} : 13%	~1.2	-0.95V	2
Oxide derived Cu dendrites	FE _{PrOH} : 13.1% CE _{PrOH} : -2.56 mA cm ⁻²	FE _{EtOH} : 10.4% CE _{EtOH} : -2.01 mA cm ⁻²	~1.3	-0.9V	3
Plasma activated Cu cubes	FE _{PrOH} : 8.1 % CE _{PrOH} : -1.8 mA cm ⁻²	FE _{EtOH} : 17 % CE _{EtOH} : -3.3 mA cm ⁻²	~0.5	-0.95V	4
Au nanoparticles on Cu foil	FE _{PrOH} : 4.5 % CE _{PrOH} : -0.7 mA cm ⁻²	FE _{EtOH} : 3 % CE _{EtOH} : -0.5 mA cm ⁻²	~1.5	-0.95V	5

Table S4. Average partial current densities of multicarbon alcohols formed over the *od*-Pd₉Cu₉₁ catalyst at different applied potentials.

E vs. RHE	j_{PrOH} (mA cm⁻²)	j_{EtOH} (mA cm⁻²)	j_{Alcohol} (mA cm⁻²)
-0.45	-0.09	-0.05	-0.14
-0.55	-0.41	-0.24	-0.65
-0.65	-1.15	-0.6	-1.78
-0.75	-1.96	-1.3	-3.26
-0.85	-2.5	-1.88	-4.3
-0.95	-2.12	-1.7	-3.78

Supplementary references

1. *D. Ren, N. T. Wong, A. D. Handoko, Y. Huang and B. S. Yeo, J. Phys. Chem. Lett., 2016, 7, 20-24.*
2. *K. Jiang, R. B. Sandberg, A. J. Akey, X. Liu, D. C. Bell, J. K. Nørskov, K. Chan and H. Wang, Nat. Catal., 2018, 1, 111-119.*
3. *M. Rahaman, A. Dutta, A. Zanetti and P. Broekmann, ACS Catal., 2017, 7, 7946-7956.*
4. *D. Gao, I. Zegkinoglou, N. J. Divins, F. Scholten, I. Sinev, P. Grosse and B. Roldan Cuenya, ACS Nano, 2017, 11, 4825-4831.*
5. *C. G. Morales-Guio, E. R. Cave, S. A. Nitopi, J. T. Feaster, L. Wang, K. P. Kuhl, A. Jackson, N. C. Johnson, D. N. Abram, T. Hatsukade, C. Hahn and T. F. Jaramillo, Nat. Catal., 2018, 1, 764-771.*